Photodissociation of 3-Bromo-1,1,1-trifluoro-2-propanol at 193 nm: Laser-Induced Fluorescence Detection of OH($v'' = 0$, J'')

Yogesh N. Indulkar,[†,‡] Hari P. Upadhyaya,[†] Awadhesh Kumar,*[,†] Suresh B. Waghmode,[‡] and Prakash D. Naik[†]

Radiation & Photochemistry Division, Bhabha Atomic Research Centre, Trombay, Mumbai-400 085, India, and Department of Chemistry, University of Pune, Ganeshkhind, Pune-411 007, India

Received: February 19, 2009; Revised Manuscript Received: June 17, 2009

Photodissociation of 3-bromo-1,1,1-trifluoro-2-propanol (BTFP) has been investigated at 193 nm, employing the laser photolysis laser-induced fluorescence technique. The nascent OH product was detected state selectively, and the energy released into translation, rotation, and vibration of the photoproducts has been measured. OH is produced mostly vibrationally cold, with a moderate rotational excitation, which is characterized by a rotational temperature of 640 ± 140 K. However, an appreciable amount of the available energy of 36.1 kcal mol^{-1} is released into translation of OH (15.1 kcal mol^{-1}). OH product has no preference for a specific spin−orbit state, $\Pi_{3/2}$ or $\Pi_{1/2}$. However, between two Λ-doublet states, Π^+ and Π^-, the OH product has a preference for the former by a factor of 2. A mechanism of OH formation from BTFP on excitation at 193 nm is proposed, which involves first the direct C−Br bond dissociation from a repulsive state ($n_{Br}\sigma^*_{C-Br}$) as a primary process. The primary product, $F_3C-CH(OH)-CH_2$, with sufficient internal energy undergoes spontaneous C−OH bond dissociation, through a loose transition state. The formation rate of OH is calculated to be 5.8×10^6 s^{-1} using Rice−Ramsperger−Kassel−Marcus unimolecular rate theory. Experimental results have been supported by theoretical calculations, and energies of various low-energy dissociation channels of the primary product, $F_3C-CH(OH)-CH_2$, have been calculated.

I. Introduction

Studies on halogenated alcohols have attracted great attention in the last two decades due to their importance in atmospheric and combustion chemistry. 3-Bromo-1,1,1-trifluoro-2-propanol (BTFP) is one of the important halogenated alcohols, since it is suggested to be a fire extinguishing agent,[1] as an alternative to Halon 1301 fire extinguisher, with its cup burner value of 4.1.[1] The extinguishing concentrations of BTFP liquid agent against hydrogen and hydrocarbon flames were 5.7 and 4.0, respectively.[1] BTFP is also used for the synthesis of some useful chemicals.[2] Since BTFP has several applications, its anthropogenic release to the atmosphere can be of some concern; the removal pathway of BTFP from the atmosphere has not been determined. It could be removed via its reaction with OH, photolysis, wet deposition, and dry deposition. In the troposphere, solar photolysis does not contribute significantly. But it will be a viable loss mechanism in the stratosphere, where the solar spectrum includes shorter wavelengths. The goals of the present work are to understand various channels of dissociation of BTFP on photoexcitation at 193 nm and energy partitioning of the available energy in the photoproducts.

The photochemistry of BTFP, particularly its photodissociation, is not reported in the literature. BTFP photodissociation is a potential source of bromine atoms and hydroxyl molecules in the atmosphere. The photodissociation of similar halogenated alcohols, 2-bromoethanol and 2-chloroethanol, at 193 nm has been studied experimentally,[3] and only one primary channel, halogen atom formation after C−X (X = Br, Cl) bond scission, was observed. The coproduct C_2H_4OH was reported to undergo secondary dissociation to produce C_2H_4 and OH. BTFP is similar to 2-bromoethanol except one hydrogen atom is replaced by a fully fluorinated methyl group. Unlike halogenated alcohols, studies on photodissociation dynamics of saturated alcohols, such as methanol,[4] ethanol,[5] 1-propanol, and 2-propanol,[6] report the O−H bond breaking to be the predominant pathway, and it is a fast dissociation on the repulsive excited state PES along the O−H coordinate. In these photodissociation studies of saturated alcohols, OH was not detected by laser-induced fluorescence (LIF). In contrast, photoexcitation of unsaturated alcohols, such as propargyl[7] and allyl[7,8] alcohols at 193 nm, which involves $\pi^* \leftarrow \pi$ electronic transition, leads to the formation of OH, as detected by LIF.

In the present work, the dynamics of OH formation from BTFP at 193 nm has been investigated by using the laser photolysis laser-induced fluorescence (LP-LIF) technique. Partitioning of the available energy among translational, rotational, and vibrational degrees of freedom of the photoproduct, the Λ-doublet distribution, and the spin−orbit population ratio of the OH fragments have been measured. We have discussed various possible mechanisms of OH formation from BTFP on excitation at 193 nm. We have also characterized some of the stable photoproducts of BTFP, employing FTIR absorption spectroscopy, and proposed mechanisms of various other channels of photodissociation of BTFP with the help of experimental results and molecular orbital (MO) calculations.

II. Experimental Section

Laser photolysis laser-induced fluorescence (LP-LIF) was used to study the photodissociation dynamics of BTFP. The setup of LP-LIF is described in detail in a previous paper.[9] Briefly, the photolysis laser is an excimer laser (Lambda Physik,

* Corresponding author, awadesh@barc.gov.in.
† Bhabha Atomic Research Centre.
‡ University of Pune.

10.1021/jp9015195 CCC: $40.75
Published on Web 07/09/2009

model Compex-102, Fluorine version) and the probe laser is a Quantel dye laser with frequency doubling and mixing modules (TDL90) pumped by a seeded neodymium-doped yttrium aluminum garnet (Nd:YAG) laser (Quantel model YAG980 E-20). The glass reactor had crossed arms at right angles with windows, allowing the pump and the probe laser beams to intersect at the center of the chamber. The detector was attached to the bottom window to view the intersection volume of the photolysis and probe lasers. It consists of a lens of focal length 50 mm (diameter = 38 mm), to collect the fluorescence, photomultiplier tube (Hamamatsu, model R-928P) to detect it, and a band-pass filter ($\lambda_{center} = 310$ nm, fwhm = 10 nm, $\%T_{310nm} = 10$) placed between the lens and the PMT to cut off the scattering from the photolysis laser. Both laser beams were unfocused and attenuated to prevent any saturation effect or multiphoton event. The fluorescence signal was gate integrated by a boxcar (SRS 250), averaged (30 laser shots), and fed into an interface (SRS 245) for analog to digital conversion. A Pentium II personal computer was used to control the scanning of the dye laser via RS232 interface, and data were collected through a general purpose interface bus (GPIB) using a control and data acquisition program.

The compound in the form of vapor was flowed through a glass reactor with a static pressure of ~50 mTorr at a flow velocity of ~10 cm/s and photolyzed by an ArF laser at 193 nm. The OH fragment was probed state selectively by exciting the $A^2\Sigma^+ \leftarrow X^2\Pi$ (0,0) transition of OH (306−309 nm) and monitoring the subsequent A → X fluorescence. All LIF excitation spectra were measured at the time delay between the pump and probe lasers of ~50 ns. The powers of the photolysis and the probe lasers were separately measured using photodiodes, and measured fluorescence excitation spectra were normalized with both the lasers' intensities. The LIF signal was found to be linearly proportional to the laser powers.

An attempt was made to measure the time-resolved IR fluorescence from the vibrationally excited products, including spin−orbit excited Br, if any, using a liquid nitrogen cooled InSb IR detector.

Fourier transform infrared (FTIR) absorption spectra were measured to check the purity of BTFP and to identify the stable photoproducts. A FTIR spectrophotometer (Bruker, model IFS 66v/S) and a glass cell fitted with a pair of ZnSe windows, filled with a known amount of BTFP (~3 Torr pressure), were used.

BTFP (96%, Aldrich) was further purified by vacuum distillation and was used after several freeze−pump−thaw cycles for photolysis and spectrum measurement.

III. Theoretical Methods

The structures of molecular species along with transition states were optimized using IBM PC compatible Gaussian 03 software[10] for a better understanding of the dynamics and the energetics of the experimentally observed photodissociation channels of BTFP. In addition to the OH channel, various other low-energy dissociation channels were also investigated from the primary product $F_3C-CH(OH)-CH_2$, employing density functional theory (DFT) at the B3LYP level, using 6-311+G(d,p) basis sets. Besides the B3LYP energy, the energies of the optimized structures were also calculated at the second-order Moller−Plesset (MP2) level of theory, using the same basis sets. The harmonic vibrational frequencies and force constants were calculated to ensure that the stationary points on the potential energy surfaces are true saddle points. All transition state (TS) structures were characterized by only one imaginary frequency and one negative eigenvalue of the force constant matrix. Time-dependent density functional theory (TD-DFT) with 6-311++G(d,p) basis sets was employed to calculate vertical excitation energies of the low-lying electronic states, and MOs were analyzed to assign each electronic transition.

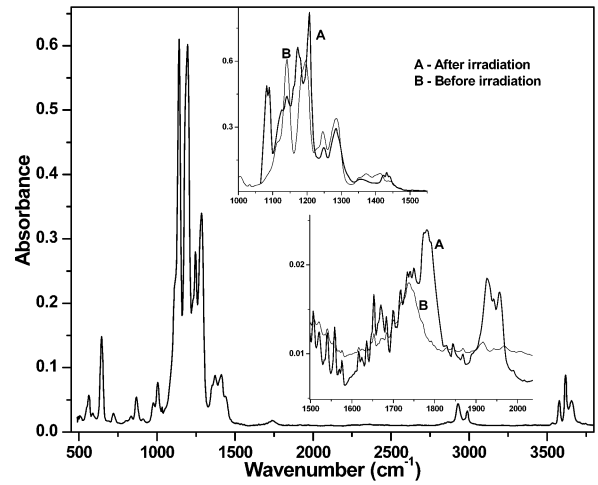

Figure 1. IR spectrum of BTFP (3 Torr) in the vapor phase using Zn−Se windows for the photolysis cell. In the inset, curve B is before irradiation and curve A is after irradiation with 900 pulses of 1 mJ of 193 nm laser photon.

IV. Results and Analysis

1. FT-IR Absorption Spectra. The IR spectrum of BTFP is hitherto unreported, so we measured the spectrum in the vapor phase, given in Figure 1, and compared it with the spectrum of 1,1,1-trifluoro-2-propanol, which is reported by National Institute of Standards and Technology (NIST). Except for differences due to the presence of bromine atom in the BTFP, its spectrum agrees well with that of 1,1,1-trifluoro-2-propanol. On photodissociation of BTFP at 193 nm, some stable products were identified, employing FT-IR absorption spectroscopy by measuring the spectra of compound before and after irradiation. New IR features in the irradiated mixture can be seen mainly between 1050 and 1100 cm^{-1} (at 1077, 1083, and 1090 cm^{-1}), between 1150 and 1220 cm^{-1} (at 1161, 1173, and 1206 cm^{-1}), and at ~1320 (broad), 1433, 1670, 1776, 1790, 1928, 1958, and 3017 cm^{-1}. Two peaks at 1817 and 1832 cm^{-1} grew after irradiating BTFP for 300 laser pulses but subsequently decreased after additional 600 pulses, implying that the corresponding product(s) undergoes further dissociation. These IR peaks reveal presence of various photoproducts, a few of these such as 1,1,1-trifluoroacetone ($F_3CC(=O)CH_3$), trifluoromethane (CF_3H), and bromotrifluoromethane (CF_3Br) were characterized using their reported IR absorption spectra.[11] Some uncharacterized bands in the spectra correspond to the products containing a carbonyl group and the C=C bond.

2. Detection of OH. The LP-LIF technique was employed to detect the transient OH radical in the photolysis of BTFP at 193 nm. Quantum state distribution of the nascent OH radicals was probed by exciting the A−X system by a frequency-doubled tunable dye laser and measuring the fluorescence generated from it. Both the (0,0) and (1,1) vibronic bands were studied and rotationally resolved lines measured for the former transition, with no signal obtained for the latter transition. This indicates that the OH radical is generated mostly in the ground vibrational level i.e., $v'' = 0$. Several rotational lines were measured for the (0,0) transition, shown in Figure 2, at 50 mTorr pressure and the time delay between the photolysis and probe lasers of 50 ns. Analyzing profiles of rotational lines of the excitation

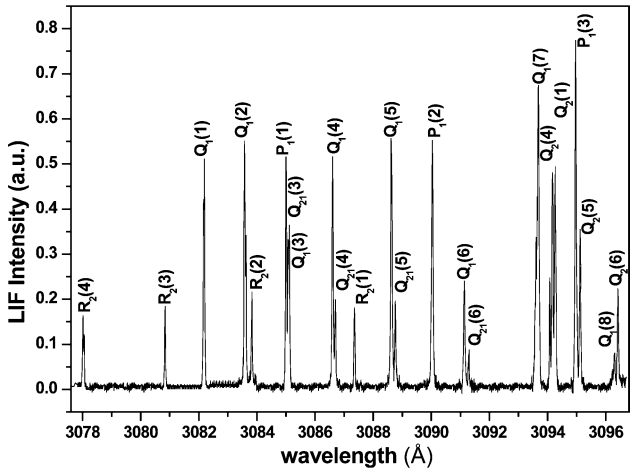

Figure 2. LIF excitation spectrum of the (0,0) band of the $A^2\Sigma^+ \leftarrow X^2\Pi$ system of the nascent OH radical formed in photodissociation of BTFP (50 mTorr) at 193 nm. Delay between pump and probe laser was 50 ns. The rotational lines are assigned in the figure.

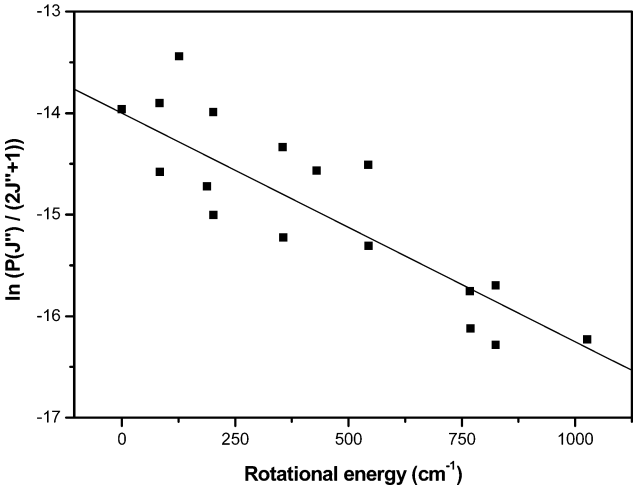

Figure 3. A Boltzmann plot of rotational state population against energy of rotational states of OH ($v'' = 0$) generated in dissociation of BTFP at 193 nm laser excitation.

spectrum, we extracted the information on dynamics of OH radical formation.

3. Average Rotational Energy of OH. Following the work of Dieke and Crosswhite,[12] the rotational lines of the (0,0) band of the $A^2\Sigma^+ - X^2\Pi$ system of the OH radical were assigned. The respective LIF intensities were normalized with respect to the photolysis and probe laser intensities, pressure of sample in the cell, and Einstein's absorption coefficients B_{ij} (taken from the work of Chidsey and Crossley[13]), to calculate the relative population of each rotational level. The corrected populations $P(J'')$ of the nascent OH fragment generated by photodissociation, were plotted against energy of rotational levels (ε), to construct a Boltzmann plot given by the equation

$$\ln \frac{P(J'')}{(2J'' + 1)} = \frac{-\varepsilon hc}{kT_R} + \text{constant} \qquad (1)$$

From the slope of this plot (Figure 3), the rotational temperature (T_R) of OH was estimated to be 640 ± 140 K, which corresponds to 1.3 ± 0.3 kcal mol^{-1} of average rotational energy into the OH fragment.

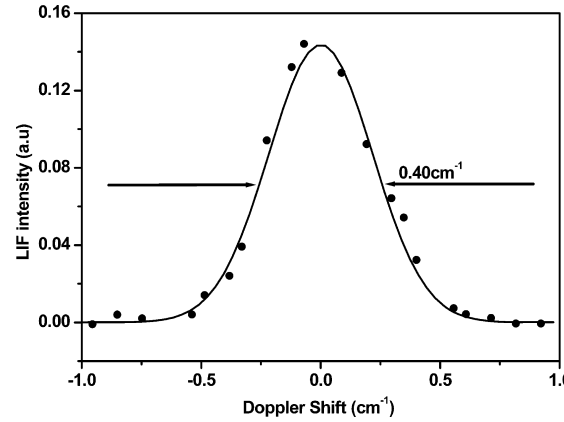

Figure 4. Doppler profile of $Q_2(6)$ line of the $A^2\Sigma^+ \leftarrow X^2\Pi$ (0,0) system of the OH radical produced in dissociation of BTFP with 193 nm laser.

4. Average Translational Energy of OH. Molecular velocity of the fragments leads to the Doppler broadening of the LIF lines. The averaged translational energy of the photoproduct OH can be estimated using widths of Doppler broadened rotational lines. The Doppler profile of the $Q_2(6)$ line of OH from BTFP is shown in Figure 4. All the rotational lines were found to have similar line widths, within the range of experimental error. After correcting the Doppler profile of the rotational lines for the probe laser line width, the linear Doppler width $\Delta\nu_D$ is related to the temperature (T_T) by the equation[14]

$$\Delta\upsilon_D = (7.16 \times 10^{-7})\upsilon_0\sqrt{T_T(\text{OH})/m_{\text{OH}}} \qquad (2)$$

where ν_0 and m_{OH} represent the center frequency of the rotational line and the mass of OH, respectively. The average translational energy in OH, $E_T(OH)$, is given by eq 3

$$E_T(\text{OH}) = \frac{3}{2}kT_T(\text{OH}) \qquad (3)$$

Ten each of $P_1(2)$ and $Q_2(6)$ lines were measured, and by use of their average line width and the temperature, the translational energy of the OH fragment was determined. For a completely isotropic velocity distribution of the OH fragment, deconvolution of the peak profiles with the instrumental functions gives the average width of 0.40 ± 0.02 cm^{-1} for Doppler broadened rotational lines. This corresponds to $E_T(OH)$ of 15.1 ± 1.8 kcal mol^{-1}.

5. Populations in Λ-Doublets and Spin−Orbit States. The Λ-doublet splitting arises due to the interaction between orbital angular momentum and nuclear rotation, and this interaction is of different strength in two Λ-doublet states, $^2\Pi^+(A')$ and $^2\Pi^-(A'')$. These states are created due to difference in the orientations of the π lobes with respect to the rotational plane of the molecule. In the Π^+ state, π lobes are parallel to the rotational plane, and the other state in which the lobes are perpendicular to the rotational plane is the Π^- state. The population in the Π^+ state is derived from the intensity of the P or R rotational lines in the excitation spectrum, and that in the second Π^- state is derived from the intensity of the Q lines. When the ratio of the corrected intensities of Q to P lines was plotted against a corresponding rotational quantum number (N''), it was found that the values were less than unity (~0.5), which is shown in Figure 5. This result indicates that the Π^+ (A′) levels

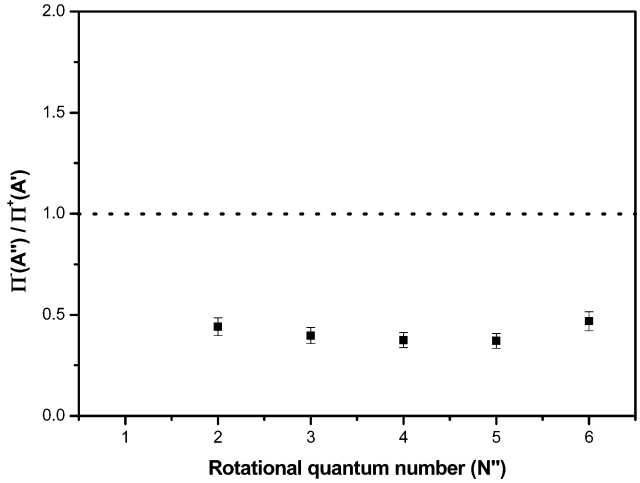

Figure 5. A plot of Λ-doublet population ratio against rotational quantum number N'' for the nascent OH formed in laser-induced photodissociation of BTFP at 193 nm. The plot indicates that the Π^+ (A′) levels are populated in preference to the Π^- (A″) levels.

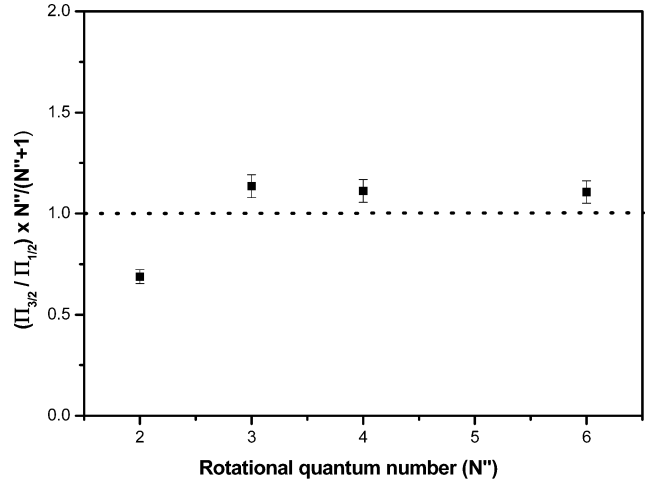

Figure 6. A plot of the spin−orbit state population distribution ratio against rotational quantum number N'' for the OH radical produced in photodissociation of BTFP with 193 nm laser. Both the spin−orbit populations are statistically produced.

are populated in preference to the Π^- (A″) levels. The measured Λ-doublet population ratio in the OH product serves as a sensitive probe both for the geometry of the reactive trajectories for a bimolecular reaction[15] and the exit channel dynamics in photodissociation.[16] The Π^-/Π^+ population smaller than 1.0 in the OH product from the H + NO_2 reaction implies that the reactive trajectories pass through the plane of the OH rotation.[15] In photodissociation this result indicates that the torque responsible for the fragment rotation lies in a preferred plane.[17,18] Thus, if dissociation proceeds through a planar configuration, it is expected to exhibit an anomalous Λ-doublet population ratio. In addition, several other dynamical effects can lead to nonequilibrium distribution of the Λ-doublet population ratio.[19] In BTFP dissociation, the transition state structure for OH formation is nonplanar; thus the planarity constraint is not expected to be responsible for the observed anomalous Λ-doublet population ratio in the OH product. Exit-channel effects,[20] which involve interactions as the fragments separate in space, can be responsible for the observed Λ-doublet population ratio in the OH product. Further, OH is produced from the primary product, $CF_3CH(OH)CH_2$ radical, which is generated impulsively involving the terminal C−Br bond scission of BTFP and expected to be highly rotationally excited. This radical, rotationally at disequilibrium, can also lead to a nonstatistical distribution of the Λ-doublet levels.

Due to spin−orbit coupling, each Π state splits into two, $\Pi_{3/2}$ and $\Pi_{1/2}$. In the case of the OH radical, the population of the $\Pi_{3/2}$ level is measured by $P_1(N'')$ or $Q_1(N'')$ or $R_1(N'')$ lines, whereas that of the $\Pi_{1/2}$ level is measured by the intensity of $P_2(N'')$ or $Q_2(N'')$ or $R_2(N'')$ lines. The ratios of corrected intensities of P_1 and P_2 lines are plotted against N'' and found that the levels are equally populated for all rotational levels up to $N'' = 6$ (Figure 6). Thus, the X $^2\Pi$ spin−orbit components ($^2\Pi_{3/2}$ and $^2\Pi_{1/2}$) of the OH product are in equilibrium. This suggests that the initially excited state of BTFP does not interact with any other triplet states, since the singlet−triplet interaction can contribute to a spin preference.

6. Formation Time of OH. The LIF intensity at the λ_{max} of different rotational lines was measured to investigate N'' dependence of the formation kinetics of OH. By selecting excitation wavelength at a particular rotational line, and scanning the time delay between the photolysis and the probe lasers, we get the temporal profile of OH formation. A plot of LIF intensity

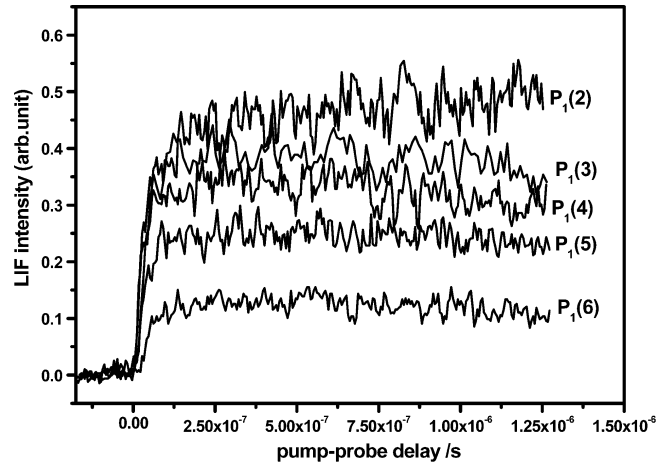

Figure 7. Formation of OH in different rotational levels (N''). The plot shows the LIF signal for $N'' = 2$, 3, 4, 5, and 6 with pump−probe time delay.

against time delay for different rotational lines is presented in Figure 7. The time delay scans show that OH formation became faster with increasing N'' from 2 to 6. This N'' dependence of formation of the OH radical is explained based on complications due to rotational relaxation from OH formed in higher N. In lower rotational levels, i.e., $N'' = 2$ or 3, apart from the population formed initially, there is increasing contribution from the relaxation of the higher rotational levels. Thus, the relaxation of higher levels to lower levels will delay the actual formation of OH directly from BTFP. Thus, the $P_1(2)$ line shows much slower formation of OH as compared to lines of higher N'', $P_1(5)$ or $P_1(6)$. Temporal evolution of $P_1(6)$, the line with highest measured value of N'', leads to the correct value of formation time of OH, and the value obtained from this line is about 50 ns. Similar N'' dependence of formation of the OH radical was observed in photodissociation of butadiene monoxide[21] at 193 nm and *o*-nitrotoluene[22] at 193 and 248 nm.

7. Theoretical Calculations. We carried out molecular orbital (MO) calculations, to investigate the potential energy surface (PES) for the OH dissociation channel, in both the ground and the excited electronic states of BTFP accessible by 193 nm laser excitation. All the structures, including the TS, have been optimized at the B3LYP/6-311+G(d,p) level. However, the TS structure for the OH formation channel could not

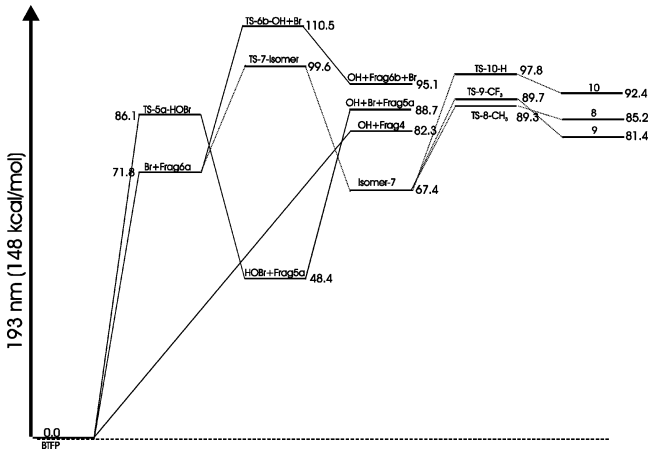

Figure 8. Relative potential energy diagram for formation of OH from the ground electronic state of BTFP on excitation at 193 nm with three different possible pathways. This figure also depicts several possible dissociation channels from the primary dissociation product $F_3C-CH(OH)-CH_2$ of BTFP. The TS structures are marked according to the reaction numbers. Details are given in the text. All energies (in kcal mol^{-1}) are at the B3LYP/6-311+G(d,p) level of theory, except TS-6b-OH which is at the MP2/6-311+G(d,p) level of theory.

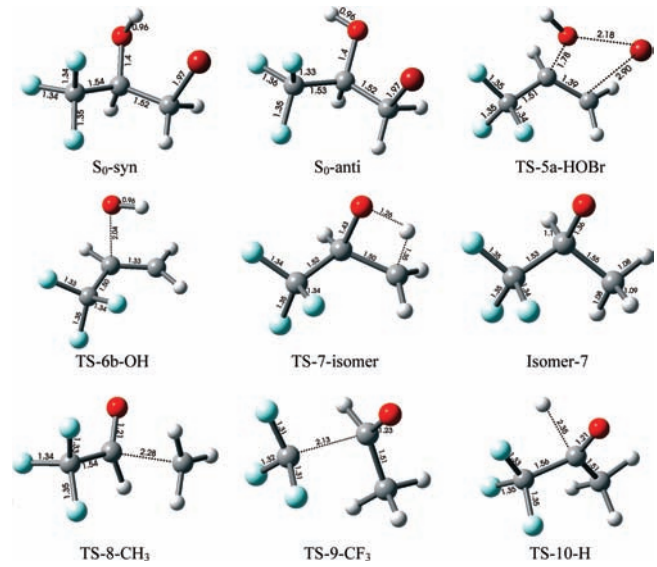

Figure 9. The optimized structures of the ground electronic state of BTFP (two conformers depicted as S_0-syn and S_0-anti) and transition states of various reactions (marked according to the reaction number followed by reaction type). All structures are optimized at the B3LYP/6-311+G(d,p) level of theory, except TS-6b-OH which is at the MP2/6-311+G(d,p) level of theory.

be optimized at this level. Therefore, the same was carried out at the MP2/6-311+G(d,p) level. All the energies used under discussion are at the B3LYP/6-311+G(d,p) level, except for the TS corresponding to OH formation, which is at the MP2/6-311+G(d,p) level. For all the radical channels studied, the projected MP2 (PMP2) energies, wherein spin contamination has been taken care of, were generally found to be lower as compared to the MP2 energies.

To check the accuracy of our energy calculations, we carried out similar calculations as the present work for the OH forming channels in 2-bromoethanol, studied by Lee and co-workers,[3] for a comparison. They predicted 68.0 and 28.0 kcal mol^{-1} for the C−Br bond energy (reaction 4 of ref 3) and the endothermicity of the secondary reaction forming OH (reaction 5 of ref 3), respectively. For the similar reaction in 2-bromoethanol, our calculations predict the C−Br bond energy to be 67.2 and 72.5(70.6) kcal mol^{-1} at the B3LYP and MP2(PMP2) levels, respectively. Similarly, we predict the endothermicity of the secondary reaction to be 25.2 and 29.1(29.3) kcal mol^{-1} at the B3LYP and MP2(PMP2) levels, respectively. Thus, our calculated energies are reasonably in good agreement with the reported values.

i. Ground Electronic State. The energy of each optimized molecular species involved in the ground electronic state photodissociation of BTFP, including transition state structures, is calculated. In Figure 8, the potential energy curves are schematically represented by indicating the energy (in kcal mol^{-1}) of each species.

Two gauche conformers of BTFP, differing in orientation of O−H with respect to C−Br have been identified. The dihedral angles for HOCBr in these two syn and anti conformers (depicted as S_0-syn and S_0-anti in Figure 9) are 6.1° and 140.2°, respectively. Between these two, syn and anti forms, the former is calculated to be more stable by about 2.1 kcal mol^{-1} (2.20 and 1.97 kcal mol^{-1} at B3LYP and MP2 level, respectively). The higher stability of the syn conformer can be attributed to an intramolecular hydrogen bond, and its evidence comes from the calculated structures. The Br···H distance in the syn form is 2.69 Å, in comparison to ∼4.0 Å in the anti form, the former is about 0.46 Å shorter than the sum of the van der Waals radii of bromine and hydrogen (3.15 Å).[23] Even the Br···O distance (3.23 Å), in the syn form is shorter than the sum of the van der Waals radii of bromine and oxygen (3.35 Å).[23] Similar intramolecular hydrogen bonds[23,24] have been observed in 2-bromoethanol and 2-chloroethanol with the added stability of about 2.0 kcal mol^{-1}.[24,25] In 2-fluoroethanol also, similar attractive fluorine−hydrogen interaction has been observed.[25,26] Thus, in BTFP also, in addition to an attractive interaction between bromine and hydrogen, an interaction between fluorine and hydrogen is expected, since the hydroxyl group and fluorine atoms (like bromine atom) are also present on the adjacent carbon atoms. However, the calculated F···H distance is 2.66 and 2.46 Å in the syn and anti forms of BTFP, respectively, in comparison to the sum of the van der Waals radii of fluorine and hydrogen of 2.55 Å.[26] Thus, the F···H interaction is not expected to be present in syn, but it is observed in anti BTFP. The syn BTFP being more stable implies that the intramolecular Br···H interaction in the syn form is stronger than the F···H interaction in the anti form.

ii. Excited Electronic State. UV−visible spectra and, in general, photochemistry of BTFP are not well studied. But these are expected to be similar to 2-bromoethanol, except for some differences arising from the presence of a CF_3 group in BTFP. Excitation at 193 nm in 2-bromoethanol is assigned to the $\sigma^*_{C-Br} \leftarrow n_{Br}$ transition.[3] In BTFP also, excitation at 193 nm is expected to lead to the same $\sigma^*_{C-Br} \leftarrow n_{Br}$ transition. The CF_3 group is not expected to produce any significant effect, since the nonbonding fluorine electrons are strongly bound. In general, the $\sigma^* \leftarrow$ n transition in alkyl halides (like in halogens and hydrogen halides) gets complicated due to a strong spin−orbit coupling of the unpaired electron remaining on the halogen atom.[27,28] Thus, because of the spin−orbit splitting of the excited state, three allowed transitions are observed, which are represented by $^1Q_1$, $^3Q_1$, and $^3Q_0$ transitions in the Mulliken notation.[29] First two transitions lead to formation of the ground state halogen atom, whereas the third transition produces the spin−orbit excited halogen atom.

We carried out population analysis to understand the nature of the excited states of BTFP. These calculations predict that

two lower transitions involve the nonbonding electrons on Br from the highest occupied molecular orbital (HOMO) and the second highest occupied molecular orbital (SHOMO), to the lowest unoccupied molecular orbital (LUMO), σ^*_{C-Br}. Thus, the $\sigma^*_{C-Br} \leftarrow n_{Br}$ transitions lead to the lowest two states, wherein the nonbonding electrons on Br are in the orbitals orthogonal to each other. Thus, excitation at 193 nm in BTFP is similar to that in bromoethanol, and it is assigned to the $\sigma^*_{C-Br} \leftarrow n_{Br}$ transition.

8. Dissociation Channels. The initial excitation at 193 nm leads to population of BTFP in a higher electronic state, which is repulsive in nature. From this state, BTFP is expected to undergo the C−Br bond cleavage impulsively, producing Br and the radical $F_3C-CH(OH)-CH_2$. This radical can dissociate subsequently to produce OH and some other observed stable products, such as $F_3C-C(=O)-CH_3$.

i. OH Formation. The observed OH photoproduct from BTFP can be ascribed to three different possible pathways (reactions 4−6), whose energetics are shown in Figure 8. The OH radical can be produced directly involving the C−OH bond cleavage (reaction 4) with the bond dissociation energy of 82.3 kcal mol^{-1}.

$$F_3C-CH(OH)-CH_2Br \rightarrow F_3C-CH-CH_2Br + OH \quad (4)$$

It can also be produced via secondary pathways (reactions 5 and 6) from primary products HOBr (reaction 5a) and $F_3C-CH(OH)-CH_2$ (reaction 6).

$$F_3C-CH(OH)-CH_2Br \rightarrow HOBr + F_3C-CH=CH_2 \quad (5a)$$

$$HOBr \rightarrow OH + Br \quad (5b)$$

$$F_3C-CH(OH)-CH_2Br \rightarrow Br + F_3C-CH(OH)-CH_2 \quad (6a)$$

$$F_3C-CH(OH)-CH_2 \rightarrow F_3C-CH=CH_2 + OH \quad (6b)$$

In reaction 5a, HOBr is eliminated from BTFP in a concerted pathway involving a four-centered TS (marked as TS-5a-HOBr in Figure 9) with an activation barrier (E_b) of 86.1 kcal mol^{-1}. Subsequently, to produce OH (reaction 5b), HOBr requires 45.3 kcal mol^{-1} of energy. The third possible pathway of OH formation is initiated by elimination of Br (reaction 6a) with bond dissociation energy of 71.8 kcal mol^{-1}, in which the cofragment further dissociates via TS (TS-6b-OH in Figure 9) with a barrier of 38.7 kcal mol^{-1} to generate OH and $F_3C-CH=CH_2$ (reaction 6b). One or more of these three mechanisms is responsible for production of OH from BTFP on excitation at 193 nm. The relative importance of these channels is discussed qualitatively in the discussion section.

ii. Other Reaction Channels. In addition to the OH channel, $F_3C-CH(OH)-CH_2$ can dissociate to produce the observed stable products, such as $F_3C-C(=O)-CH_3$. Recently, in a theoretical work on reaction of OH with propene,[30] various dissociation channels have been suggested from an intermediate $H_3C-CH(OH)-CH_2$. In the present work, the intermediate radical $F_3C-CH(OH)-CH_2$ being similar to $H_3C-CH(OH)-CH_2$, we have investigated some low-energy channels, similar to the above referred work, to explain mechanisms of formation of some observed stable products. The intermediate radical can isomerize to $F_3C-CH(O)-CH_3$ (reaction 7) through TS (TS-7-isomer in Figure 9), with E_b of 27.8 kcal mol^{-1}, which can undergo the $C-CH_3$, the $C-CF_3$ and the (O)C−H bond cleavages, respectively, to produce F_3C-CHO with CH_3 (reaction 8, E_b = 21.9 kcal mol^{-1}), H_3C-CHO with CF_3 (reaction 9, E_b = 22.3 kcal mol^{-1}), and $F_3C-C(=O)-CH_3$ with H (reaction 10, E_b = 30.4 kcal mol^{-1}), respectively.

$$F_3C-CH(OH)-CH_2 \rightarrow F_3C-CH(O)-CH_3 \quad (7)$$

$$F_3C-CH(O)-CH_3 \rightarrow F_3C-CHO + CH_3 \quad (8)$$

$$\rightarrow H_3C-CHO + CF_3 \quad (9)$$

$$\rightarrow F_3C-C(=O)-CH_3 + H \quad (10)$$

Structures of various stable molecular species and transition states have been calculated to investigate the energetics of these channels. The optimized transition state structures involved in the reaction channels (reactions 7−10) are shown in Figure 9; the corresponding energies are given in Figure 8.

Another possible precursor to the stable product $F_3C-C(=O)CH_3$ can be BTFP in the ground electronic state with sufficient internal energy. This mechanism is possible (but less likely), if a fraction of the electronically excited BTFP relaxes to the ground electronic state, in addition to undergoing the C−Br bond cleavage. 1,2-Elimination of HBr (reaction 11a), the lowest energy dissociation channel from the ground electronic state of BTFP, can produce the cofragment, $F_3C-C(OH)=CH_2$, which can further rearrange (reaction 11b) to its more stable keto form, $F_3C-C(=O)-CH_3$, involving a four-centered TS.

$$F_3C-CH(OH)-CH_2Br \rightarrow HBr + F_3C-C(OH)=CH_2 \quad (11a)$$

$$F_3C-C(OH)=CH_2 \rightarrow F_3C-C(=O)-CH_3 \quad (11b)$$

V. Discussion

1. Mechanism of OH Formation. To explain the formation of the OH radical from BTFP on excitation at 193 nm, three different plausible mechanisms (reactions 4−6) have been proposed. Theoretical studies indicate that lower excited electronic states of BTFP are repulsive in nature with respect to the C−Br bond, and hence the C−Br bond dissociation leading to Br (reaction 6a) is expected to be the most facile primary dissociation channel. Further, the ground state calculations estimate the bond dissociation energy for the C−Br bond to be 71.8 kcal mol^{-1}. Thus, taking these facts into account, direct elimination of OH (reaction 4) with a higher barrier of 82.3 kcal mol^{-1} appears to be less likely. Similarly, another possible pathway for OH formation (reaction channel 5) also has a higher barrier (86.1 kcal mol^{-1}) for formation of HOBr, an expected precursor to OH. Thus, the mechanism of OH formation from BTFP involves first a Br elimination, followed by fragmentation of the coproduct radical, which is unstable with respect to OH and $F_3C-CH=CH_2$ (reaction 6a). The corresponding TS structure (marked as TS-6b-OH in Figure 9) is calculated, in which the C−OH bond is extended to 2.04 Å. This proposed mechanism of OH formation from BTFP is similar to that from similar alcohols,[3] 2-bromoethanol and 2-chloroethanol, where

OH was proposed to be generated from a primary product H_2C-CH_2OH (produced after Br elimination), from which a fraction with higher energy undergoes dissociation to produce OH and C_2H_4. These products showed a high degree of anisotropy in their angular distribution, with OH and C_2H_4 peaking strongly forward and backward with respect to the initial C−Br recoil direction. Lee and co-workers[3] pointed out that in the photodissociation of 2-bromoethanol, the secondary angular distribution of OH and C_2H_4 with respect to the initial BrC_2H_4OH velocity vector will result in an isotropic center-of-mass (c.m.) angular distribution, since the primary C_2H_4OH product was found to be long-lived with respect to its rotational period. Moreover, the forward−backward peaking of the secondary products is with respect to the C_2H_4OH velocity vector. Similar isotropic c.m. angular distribution of products, OH and its cofragment, from BTFP on excitation at 193 nm is expected, since the proposed mechanism of OH formation is similar and formation of OH is measured to be relatively slow (∼50 ns). However, we could not measure the angular distribution of the products, since we currently lack the required facility.

2. Partitioning of the Available Energy. The energy available to the primary products of reaction 6a, $E_{avl}(6a)$ is given as

$$E_{avl}(6a) = h\nu - \Delta E(6a) = 148 - 71.8 = 76.2 \text{ kcal mol}^{-1} \quad (12)$$

where $h\nu$ is the energy corresponding to 193 nm photon and $\Delta E(6a)$ is the endothermicity of the reaction. Similarly, the energy available to the secondary products of reaction 6b is given as

$$E_{avl}(6b) = E_{avl}(6a) - \Delta E(6b) - E_T(6a) = (76.2 - 23.3) \text{ kcal mol}^{-1} - E_T(6a) \quad (13)$$

where $\Delta E(6b)$ and $E_T(6a)$ are the endothermicity of reaction 6b and the average amount of energy released into translation in reaction 6a, respectively. Using 22% of the available energy (discussed vide infra) appearing as $E_T(6a)$ in BTFP, $E_{avl}(6b)$ is 36.1 (52.9 − 16.8) kcal mol^{-1}.

OH is produced as a secondary product in the reaction 6b from the primary product $F_3C-CH(OH)-CH_2$. The OH translational energy $E_T(OH)$ is measured to be 15.1 kcal mol^{-1}, which implies the total translational energy release$E_T(Total)$, in the two-step dissociation process of BTFP to be 17.8 kcal mol^{-1} (using eq 14)

$$E_T(\text{Total}) = E_T(\text{OH})\left[1 + \frac{m_{OH}}{m_{coproduct}}\right] \quad (14)$$

where m_{OH} and $m_{coproduct}$ are masses of OH and its coproduct ($CF_3CH{=}CH_2$), respectively. In this case it is assumed that the velocity of the primary product $F_3C-CH(OH)-CH_2$ relative to the parent center-of-mass is zero, implying that all of the OH translational energy is derived from the secondary C−O bond scission. Since the primary dissociation process occurs on a repulsive surface of BTFP on excitation at 193 nm, velocity of the coproduct is not zero. Dissociation from a repulsive surface implies the impulsive mechanism of the energy partitioning, and hence it will lead to an appreciable amount of energy released in the relative translation of primary products. To estimate the total translational energy release, $E_T(Total)$ in this case of two-step three-body dissociation of BTFP, we have followed similar methodology as Guest and co-workers[31] for the acetic acid dissociation, and derived $E_T(Total)$ as follows

$$E_T(\text{Total}) = E_T(\text{OH})\left[1 + \frac{m_{OH}}{m_{coproduct}}\right] + E_T(\text{Rad})\left[\frac{m_{coproduct}}{m_{Rad}} + \frac{m_{Rad}}{m_{Br}} - \frac{m_{OH}^2}{m_{coproduct}m_{Rad}}\right] \quad (15)$$

where m_{Rad} and m_{Br} are masses of the radical $F_3C-CH(OH)-CH_2$ and Br, respectively, and $E_T(Rad)$ is the translational energy of the radical. For determination of $E_T(Total)$ using this relation, only $E_T(Rad)$ is unknown, which we have not measured. Since this primary dissociation process occurs on a repulsive surface, we estimated this value to be 6.9 kcal mol^{-1} with total translational energy release in reaction 6a to be 16.8 kcal mol^{-1} (22% of the available energy), using the soft impulsive model[32] of energy partitioning. With the above estimated value of $E_T(Rad)$ = 6.9 kcal mol^{-1}, $E_T(Total)$ is evaluated to be 33.2 kcal mol^{-1}. The evaluated translational energy release (22%) in the primary reaction of BTFP is lower than the measured values of the same in 2-bromoethanol.[3] An average of 42% and 31% of the available energy is reported to be released in translation of the primary products of the C−Br bond dissociation in 2-bromoethanol ($1,2\text{-}C_2H_4BrOH$)[3] and $1,2\text{-}C_2F_4BrI$[28] at 193 nm, respectively. A probable explanation for the lower amount of energy into translation in the latter, with almost the same C−Br bond strength, was given based on greater number of low-frequency vibrational modes in the C_2F_4I product.

OH is produced mostly in the vibrational ground state ($v'' = 0$) with moderate rotational excitation of 1.3 kcal mol^{-1} on photoexcitation of BTFP at 193 nm. But, an average of 33.2 kcal mol^{-1} of the available energy (52.9 kcal mol^{-1}) is released into translation of reaction 6, implying the balance 18.4 (52.9 − 33.2 − 1.3) kcal mol^{-1} of energy is available for the internal energy of $F_3C-CH{=}CH_2$, the coproduct of OH, in reaction 6b, assuming spin−orbit excited Br is not produced. Thus, a significant fraction of the available energy in the two-step three-body dissociation process is released in translation ($f_T \sim 0.60$), mainly because the primary reaction occurs on a repulsive surface and the secondary reaction has an exit barrier.

Bond dissociation energies, used for evaluating the amount of available energy, are theoretically calculated. Similarly, the translational energy release in the primary reaction is estimated employing the impulsive dissociation. Therefore, a high level of theoretical calculations for energies to increase the accuracy and the experimental measurement of the translational energy release in the primary dissociation channel involving the C−Br bond scission can increase the accuracy of estimate of the available energy, which will result in improved evaluation of energies in the relative translation and the internal states of the products. However, it is evident that a significant part (∼60%) of the available energy is released as the translational energy of the products.

A relatively high fraction of the available energy release into the relative translation suggests that either the C−OH bond dissociation (reaction 6b) takes place impulsively from a repulsive state of $F_3C-CH(OH)-CH_2$ or there exists an exit barrier in the OH channel. Although the primary C−Br bond

scission is impulsive, the possibility of the impulsive mechanism for the secondary dissociation of the C−OH bond is discounted both experimentally and theoretically. The impulsive mechanism should lead to fast formation of OH, within the photolysis laser pulse of 20 ns. However, we observed the slow formation of OH with a risetime of ∼50 ns. We further verified the slow formation of OH by calculating its formation rate, from the primary product $F_3C-CH(OH)-CH_2$ with the internal energy of 59.4 kcal mol^{-1}, which is $E_{avl}(6a) - E_T(6a)$, to be 5.8 × 10^6 s^{-1}, using RRKM (Rice−Ramsperger−Kassel−Marcus) unimolecular theory.[33,34] The RRKM rate is about 3.5 times lower than the measured value of ∼2.0 × 10^7 s^{-1}. Since all the required input parameters, rotational constants, vibrational frequencies, and the activation barrier, are theoretically evaluated values, such discrepancies in the measured and the calculated rates are not surprising and may be considered in good agreement. The second possibility of the presence of an exit barrier in the C−OH bond scission, producing OH, can be validated through the proposed mechanism of OH formation (reaction 6a). Our calculations support this proposed mechanism by showing presence of the expected exit barrier, which is 10.0(1.9) kcal mol^{-1} at MP2(PMP2)/6-311+G(d,p) level of theory. However, Figure 8 does not show this correct value of the exit barrier, since in the figure the energy of the TS is at the MP2/6-311+G(d,p) level and that of the products is at the B3LYP/6-311+G(d,p) level. Thus, the calculated value of the exit barrier is in agreement with the observed exit barrier value of 5−7 kcal mol^{-1} in dissociation of 2-bromoethanol and 2-chloroethanol on excitation at 193 nm.[3] Thus, the presence of an exit barrier is mainly responsible for release of a substantial amount of the available energy in relative translation in the secondary reaction (C−OH dissociation channel).

Photodissociation dynamics of BTFP at 193 nm appears to be similar to that of 2-bromoethanol.[3] OH is produced as a secondary product, following direct C−Br bond dissociation from a repulsive surface. The translational energy release in the primary reaction step of 2-bromoethanol is reported to be about 42% of the available energy. Although we could not measure the translational energy release in the above step in the case of BTFP dissociation, it is expected to be high due to the repulsive nature of the surface, and the same was estimated to be 22% of the available energy using a soft impulsive model (as discussed earlier). Even in the secondary reaction of BTFP producing OH, an appreciable amount of energy is released into translation. The presence of the CF_3 group in BTFP does not play any significant role in its photochemistry with respect to OH formation at 193 nm, since the nonbonding electrons on fluorine atoms do not participate in excitation at 193 nm. Even our CIS level excited state calculations amply demonstrate nonparticipation of nonbonding electrons on fluorine in prepared excited states of BTFP.

In alkyl halides and haloalcohols it is interesting to answer whether halogen is produced in the ground or the spin−orbit excited state. This measurement on BTFP can provide some information on the contributions of the three excited states to the $\sigma^* \leftarrow$ n transition at 193 nm. In addition, it will help in evaluating correctly the available energy to the secondary products. We could not detect any IR emission from the excited Br ($^2P_{1/2}$) at 2.71 μm, implying that Br is produced mostly in the ground spin−orbit state ($^2P_{3/2}$). This result suggests that excitation of BTFP at 193 nm leads to mainly $^1Q_1$ and $^3Q_1$ transitions. We plan to employ a more sensitive resonance-enhanced multiphoton ionization technique to detect the excited Br, if it is produced in small yields.

VI. Conclusions

3-Bromo-1,1,1-trifluoro-2-propanol (BTFP) undergoes photodissociation on excitation at 193 nm to produce OH($v'' = 0$, J''). OH is produced as a secondary product from the primary product $F_3C-CH(OH)-CH_2$, formed by a direct C−Br bond dissociation from a repulsive surface. Measurements on the nascent state population distribution of OH reveal that it is produced mostly in the vibrationally ground state ($v'' = 0$), with its rotational population being characterized by a rotational temperature of 640 ± 140 K. However, a significant amount of the available energy (36.1 kcal mol^{-1}) of the secondary reaction is released as the translational energy of OH (15.1 kcal mol^{-1}), mainly because the C−OH bond dissociation reaction has an exit barrier. Our theoretical calculations predict this barrier to be about 10.0(1.9) kcal mol^{-1} at MP2(PMP2)/6-311+G(d,p) level of theory. In addition to the OH channel, several other pathways are available from the primary product $F_3C-CH(OH)-CH_2$, on excitation of BTFP at 193 nm.

Acknowledgment. We thank Dr. P. N. Bajaj, Dr. S. K. Sarkar, and Dr. T. Mukherjee for their constant support and encouragement.

References and Notes

(1) Knutsen, L.; Morrey, E.; Riches, J. *Halon Options Technical Conference, 24−26 April*, 2001; p 235.
(2) Haas, H. C.; Schuler, N. W. *J. Polym. Sci., Part A* **1964**, *2*, 1641.
(3) Hintsa, E. J.; Zhao, X.; Lee, Y. T. *J. Chem. Phys.* **1990**, *92*, 2280.
(4) Harich, S.; Lin, J. J.; Lee, Y. T.; Yang, X. *J. Phys. Chem. A* **1999**, *103*, 10324.
(5) Xu, K.; Amaral, G.; Zhang, J. *J. Chem. Phys.* **1999**, *111*, 6271.
(6) Zhou, W.; Yuan, Y.; Zhang, J. *J. Chem. Phys.* **2003**, *119*, 7179.
(7) Dhanya, S.; Kumar, A.; Upadhyaya, H. P.; Naik, P. D.; Saini, R. D. *J. Phys. Chem. A* **2004**, *108*, 7646.
(8) Kang, T. Y.; Shin, S. K.; Kim, H. L. *J. Phys. Chem. A* **2003**, *107*, 10888.
(9) Naik, P. D.; Upadhyaya, H. P.; Kumar, A.; Sapre, A. V.; Mittal, J. P. *J. Photochem. Photobiol.: Photochem. Rev.* **2003**, *3*, 165.
(10) Frisch, M. J.; Trucks, G. W.; Schlegel, H. B.; Scuseria, G. E.; Robb, M. A.; Cheeseman, J. R.; Montgomery, J. A., Jr.; Vreven, T.; Kudin, K. N.; Burant, J. C.; Millam, J. M.; Iyengar, S. S.; Tomasi, J.; Barone, V.; Mennucci, B.; Cossi, M.; Scalmani, G.; Rega, N.; Petersson, G. A.; Nakatsuji, H.; Hada, M.; Ehara, M.; Toyota, K.; Fukuda, R.; Hasegawa, J.; Ishida, M.; Nakajima, T.; Honda, Y.; Kitao, O.; Nakai, H.; Klene, M.; Li, X.; Knox, J. E.; Hratchian, H. P.; Cross, J. B.; Adamo, C.; Jaramillo, J.; Gomperts, R.; Stratmann, R. E.; Yazyev, O.; Austin, A. J.; Cammi, R.; Pomelli, C.; Ochterski, J. W.; Ayala, P. Y.; Morokuma, K.; Voth, G. A.; Salvador, P.; Dannenberg, J. J.; Zakrzewski, V. G.; Dapprich, S.; Daniels, A. D.; Strain, M. C.; Farkas, O.; Malick, D. K.; Rabuck, A. D.; Raghavachari, K.; Foresman, J. B.; Ortiz, J. V.; Cui, Q.; Baboul, A. G.; Clifford, S.; Cioslowski, J.; Stefanov, B. B.; Liu, G.; Liashenko, A.; Piskorz, P.; Komaromi, I.; Martin, R. L.; Fox, D. J.; Keith, T.; Al-Laham, M. A.; Peng, C. Y.; Nanayakkara, A.; Challacombe, M.; Gill, P. M. W.; Johnson, B.; Chen, W.; Wong, M. W.; Gonzalez, C.; Pople, J. A. *Gaussian 03, Revision C.02*; Gaussian Inc.: Wallingford, CT, 2004.
(11) Pouchert, C. J. *The Aldrich library of FT-IR spectra*, 1st ed.; Aldrich Chemical Co., Inc.: Milwaukee, WI, 1989; Vol. 3, Vapor Phase.
(12) Dieke, G. H.; Crosswhite, H. M. *J. Quant. Spectrosc. Radiat. Transfer* **1961**, *2*, 97.
(13) Chidsey, I. L.; Crossley, D. R. *J. Quant. Spectrosc. Radiat. Transfer* **1980**, *23*, 187.
(14) Demtroder, W. *Laser spectroscopy*; Springer: New Delhi, 2004.
(15) Mariella, R. P.; Lantzsch, B.; Maxson, V. T.; Luntz, A. C. *J. Chem. Phys.* **1978**, *69*, 5411.
(16) Dixon, R. N. *J. Chem. Phys.* **1995**, *102*, 301.
(17) Andresen, P.; Ondrey, G. S.; Titze, B.; Rothe, E. W. *J. Chem. Phys.* **1984**, *80*, 2548.
(18) Vasudev, R.; Zare, R. N.; Dixon, R. N. *J. Chem. Phys.* **1984**, *80*, 4863.
(19) Wurps, H.; Spiecker, H.; ter Meulen, J. J.; Andresen, P. *J. Chem. Phys.* **1996**, *105*, 2654.
(20) Pavlov-Verevkin, V. B.; Lorquet, J. C. *J. Chem. Phys.* **2005**, *123*, 074324.

(21) Sengupta, S.; Indulkar, Y.; Kumar, A.; Naik, P. D.; Bajaj, P. N. *J. Chem. Phys.* **2008**, *128*, 024309.
(22) Sengupta, S.; Upadhyaya, H. P.; Kumar, A.; Dhanya, S.; Naik, P. D.; Bajaj, P. N. *Chem. Phys. Lett.* **2008**, *452*, 239.
(23) Azrak, R. G.; Wilson, E. B. *J. Chem. Phys.* **1970**, *52*, 5299.
(24) Buckley, P.; Giguere, P. A.; Schneider, M. *Can. J. Chem.* **1969**, *47*, 901.
(25) Wilberg, K. B.; Murcko, M. A. *J. Mol. Struct. (THEOCHEM)* **1988**, *163*, 1.
(26) Buckton, K. S.; Azrak, R. G. *J. Chem. Phys.* **1970**, *52*, 5652.
(27) Pence, W. H.; Baughcum, S. L.; Leone, S. R. *J. Phys. Chem.* **1981**, *85*, 3844.
(28) Krajnovich, D.; Butler, L. J.; Lee, Y. T. *J. Chem. Phys.* **1984**, *81*, 3031.
(29) Mulliken, R. S. *J. Chem. Phys.* **1940**, *8*, 382.
(30) Huynh, L. K.; Zhang, H. R.; Zhang, S.; Eddings, E.; Sarofim, A.; Law, M. E.; Westmoreland, P. R.; Truong, T. N. *J. Phys. Chem. A* **2009**, *113*, 3177.
(31) Hunnicutt, S. S.; Waits, L. D.; Guest, J. A. *J. Phys. Chem.* **1991**, *95*, 562.
(32) Tuck, A. F. *J. Chem. Soc., Faraday Trans. 2* **1977**, *73*, 689.
(33) Gilbert, R. G.; Smith, S. C.; Jordan, M. J. T. *UNIMOL program suite*, 1993.
(34) Gilbert, R. G.; Smith, S. C. *Theory of Unimolecular and Recombination Reactions*; Blackwell Scientific Publications: Oxford and Cambridge, 1990.

JP9015195